# PERSULFATE ACTIVATION-INDUCED DEGRADATION OF AQUEOUS METHYL ORANGE CATALYZED BY CuO/MnO2 MIXED METAL OXIDES

ISSN (print): 1859-4433; (online): 2615-9635

Do Huynh Dong Thu<sup>(1)</sup>, Ngo Minh Hieu<sup>(1)</sup>, Nguyen Le Bach Diep<sup>(1)</sup>, Huynh Thi Nha Truc<sup>(1)</sup>, Le Nguyen Hai Hung<sup>(1)</sup>, Nguyen Trung Hieu<sup>(1)</sup>

(1) Thu Dau Mot University
Corresponding author: hieunt@tdmu.edu.vn

DOI: 10.37550/tdmu.EJS/2025.03.671

#### Article Info

## Volume: 7 Issue: 3 Sep: 2025

**Received:** Jul. 9<sup>th</sup>, 2025 **Accepted:** Sep. 3<sup>rd</sup>, 2025 **Page No:** 723-733

# Abstract

MnO2 has the advantage of being environmentally friendly and abundant in soil, but its ability to activate persulfate is poor. This study combines MnO2 with CuO into a mixed metal oxide through a one-step reaction to increase the persulfate activation efficiency of the obtained product. These mixed oxides were synthesized by alkalization of a solution containing ions of two metals and then calcined at 300°C. The obtained oxide catalysts were characterized by methods such as FTIR, SEM, BET analysis, and zeta potential. The adsorption and decomposition of methyl orange (MO) were experimentally conducted in batch form using the above mixed metal oxides as adsorbents or persulfate activators. The results showed that the mixed oxides exhibited characteristic peaks in the FTIR spectrum, and were in the form of nanorods (CuO) and amorphous small particles (3:1CuO/MnO2). The CuO catalyst has a specific surface area of 20.23m<sup>2</sup>/g and pore sizes ranging from 20 to 30Å. The zeta potentials of both CuO and MO were highly negative, e.g., -46.5mV and -24.1mV, respectively. The adsorption capacities of MO onto the mixed oxides were quite low (~13.5%) and decreased gradually as the CuO content decreased. However, the persulfate activation capacity of the mixed oxides for MO decomposition was quite high, e.g., that of 3:1CuO/MnO2 for 40mg/L MO was 74.1%. In addition, the decomposition of MO almost followed pseudo-second-order reaction kinetics.

Keywords: CuO, methyl orange, mixed metal oxide, MnO2, persulfate activation

## 1. Introduction

Conventional processes for dye wastewater treatment, such as physical adsorption, chemical coagulation, and biodegradation, often face significant challenges, including incomplete dye removal, generation of secondary pollutants, and high operating costs. These methods may not effectively remove persistent organic dyes, leading to long-term environmental pollution. In contrast, Cu-Mn-O mixed oxide catalysts are a promising

ISSN (print): 1859-4433; (online): 2615-9635

solution that not only adsorbs dyes but also facilitates persulfate-activated degradation of these compounds. This dual-action process ensures more thorough treatment without the risk of generating harmful secondary pollutants.

Persulfate-based advanced oxidation processes (AOPs) have gained significant attention for treating persistent pollutants, thanks to the strong oxidizing ability of sulfate radicals (SO<sub>4</sub>•¬), their long half-life, broad effective pH range (3-11), and the practicality of persulfate storage and transport (Wang & Wang, 2022). However, since persulfate alone has limited oxidizing capacity, selecting an effective activation method is essential to enhance its performance (Zhi et al., 2020). Various activation strategies have been developed, including thermal, UV, microwave, ultrasonic, alkaline, electrochemical, carbon-based, and transition metal-based methods. Among these, heterogeneous catalysts containing transition metals offer notable advantages: they require no external energy input, function across a wide pH range, are easy to scale up, and can be separated and reused after treatment (Oyekunle et al., 2022). Catalysts incorporating metals such as Co, Ni, Fe, Mn, Cu, and Ru have shown strong potential for persulfate activation. In particular, manganese-based catalysts have attracted growing interest due to their low toxicity, environmental compatibility, abundant natural availability, and multivalent redox properties (Zhu et al., 2020).

It has been demonstrated that oxides containing manganese, including manganese tetroxide, manganese trioxide, α-manganese dioxide, and β-manganese dioxide, are efficient persulfate catalysts (Huang & Zhang, 2019). Specifically, the benefits of α-MnO<sub>2</sub> are its abundance in soils, environmental friendliness, and structural stability (Zhao et al., 2022). Nevertheless, it is prone to deactivation and has poor efficiency. The Mn<sup>3+</sup>/Mn<sup>4+</sup> cycle can be made more efficient by combining α-MnO<sub>2</sub> with other metal oxides (Wu et al., 2023). Improved catalytic efficiency over single metal oxides is the result of both an increase in specific surface area and an increase in the rate of electron transport between active sites at the interface of the two oxides (Liu et al., 2020). Recent studies have shown that modifying manganese dioxide with copper can significantly improve its catalytic performance. For instance, researchers created a mesoporous Cu/MnO<sub>2</sub> material that outperformed both pure MnO<sub>2</sub> and CuO in Fenton-like reactions. This enhanced activity was mainly due to the efficient decomposition of hydrogen peroxide and the redox cycling between manganese and copper ions (Yang et al., 2021). The presence of benzotriazole ligands on the copper surface further boosted surface oxidation by interacting with Mn<sup>4+</sup>. In a related study, copper doping in amorphous MnO<sub>2</sub> was found to increase the Mn<sup>4+</sup>/Mn<sup>3+</sup> ratio, generate more oxygen vacancies, and improve crystallinity. These changes accelerated redox cycling and helped activate peroxymonosulfate (PMS), leading to more effective degradation of organic pollutants like phenol. A free-standing α-MnO<sub>2</sub>@CuO membrane with a layered nanostructure has been successfully used to activate PMS for the oxidative degradation of organic dyes in water, demonstrating excellent catalytic efficiency (Luo et al., 2018). However, this MnO<sub>2</sub>@CuO catalyst was prepared through a step-by-step process, in which MnO<sub>2</sub> and CuO were synthesized separately and combined through a phase interface. To simplify the process and potentially improve catalytic performance, the present study focused on synthesizing a Cu-Mn-O mixed oxide in a single step. This approach aimed to create a more integrated material and investigate how the one-step synthesis method influences the catalytic activity of the resulting mixed metal oxide.

#### 2. Materials and methods

#### 2.1. Materials

Ammonium persulfate ( $(NH_4)_2S_2O_8, \ge 99\%$ ), sodium hydroxide (NaOH, > 96%), copper (II) chloride dihydrate ( $CuCl_2.2H_2O$ , 99%), trisodium citrate dihydrate ( $Na_3C_6H_5O_7.2H_2O$ , 99%), manganese (II) sulfate monohydrate ( $MnSO_4.H_2O$ , 99%), methyl orange (99%), polyethylene glycol (PEG, 400 Da), ethanol ( $C_2H_5OH$ , 99%) were provided by Xilong Scientific. Chemicals were used as received without any further purifications, and distilled water was used.

#### 2.2. Method

# 2.2.1. Oxide catalyst preparation

The metal salts of Cu(II) and Mn(II) with Cu:Mn molar ratios of 0:1, 3:1, 1:1, 1:3, and 1:0 and 1.0mL of PEG-400 (for ratio of 1:0) or 1.0g of citrate salt (for other ratios) were dissolved with 400mL of distilled water to form a solution and heated at 70-80°C. Then, a certain amount of excess NaOH dissolved in 50mL of distilled water was slowly dropped into the metal salt solution and stirred, while continuing to gently heat the mixture at 70-80°C for 2-3 hours. The solid precipitate was filtered off, washed several times with water, washed again with ethanol, and dried at 70°C for 24 hours. Finally, the solid product was calcined at 300°C for about 3 hours. The obtained product was characterized by FTIR (Fourier transform infrared spectroscopy), BET (Brunauer–Emmett–Teller) analysis, SEM (scanning electron microscope), and zeta potential.

## 2.2.2. Dye adsorption and degradation experiment

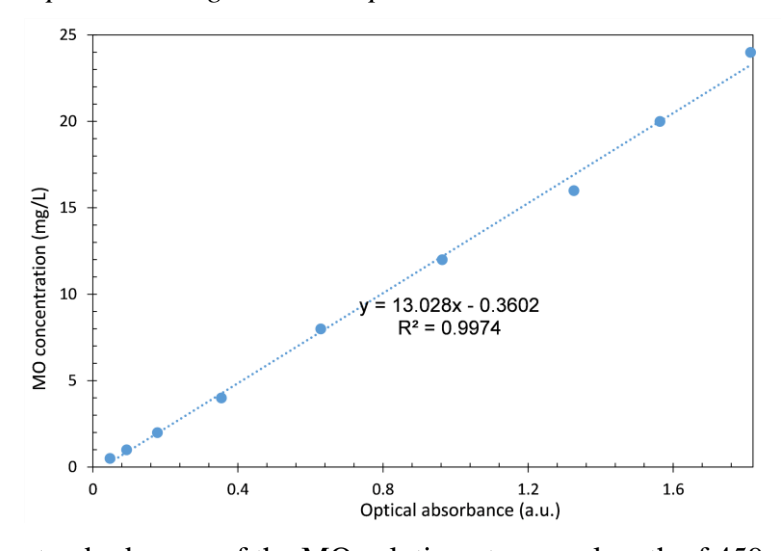


Figure 1. The standard curve of the MO solution at a wavelength of 459nm

150ml of methyl orange (MO) dye with a certain concentration (10-40mg/L) was put into a 250mL beaker placed on a magnetic stirrer equipped with a magnetic bar. Then, 0.04g of catalyst was added, and the adsorption experiment started. At the times of 3, 5, 8, 15, 30, 60, 90, and 120 minutes, 5mL of the above mixture was withdrawn into a test tube and centrifuged at 6000 rpm for 5 minutes. Then, the clear solution in the test tube was measured for optical absorption at a wavelength of 459nm on a UVmini-1240 spectrophotometer. For the MO decomposition experiment, the steps were similar to the above, but 0.02g of ammonium persulfate was added to the dye solution along with the catalyst. The MO removal efficiency was determined by the following equation:

$$\%R = \frac{C_0 - C_t}{C_0} \times 100\%$$
 (1)

Where %R is the dye removal rate,  $C_0$  is the initial dye concentration (mg/L), and  $C_t$  is the dye concentration at time t.

#### 3. Result and discussion

## 3.1. Materials characterization

# 3.1.1. FTIR of prepared catalyst

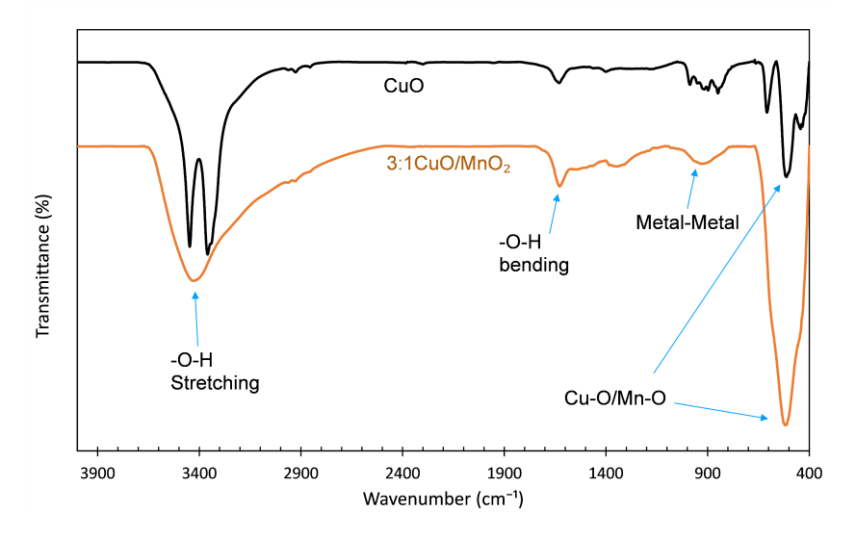


Figure 2. FTIR spectra of prepared CuO and 3:1CuO/MnO<sub>2</sub>.

FTIR spectra of CuO and the 3:1CuO/MnO<sub>2</sub> mixed oxide showed differences, indicating that there were interactions between the two oxides. The CuO spectrum displayed characteristic absorption peaks of -O-H stretching and bending vibrations (around 3400cm<sup>-1</sup> and 1600cm<sup>-1</sup>) and some sharp peaks for Cu-O stretching vibrations below 600cm<sup>-1</sup> (Fernandes et al., 2009). When mixed with MnO<sub>2</sub>, the spectrum of the mixed material retained the characteristic vibrations of the -O-H group but with reduced intensity and broader peaks. More importantly, the characteristic metal-metal peak appeared more clearly at 1000-1100cm<sup>-1</sup> and the significant change in the Cu-O/Mn-O region below 700cm<sup>-1</sup> (the peak became broader, less sharp, and more intense), indicating the formation of new bonds between Cu and Mn. This confirms chemical interaction and mixed oxide formation rather than physical mixing.

## 3.1.2. SEM of metal oxide catalyst

Figures 3 and 4 show a clear difference in morphology between CuO and the 3:1CuO/MnO<sub>2</sub> mixed oxide. The CuO particles (Figure 3) exhibit a fairly uniform rod-like morphology(Chang & Zeng, 2004) with a length of about 100nm and a width of about 30nm. In contrast, the 3:1CuO/MnO<sub>2</sub> mixed oxide (Figure 4) shows a structure without a clearly defined shape, which appears to be amorphous particles of very small size and quite uniformly dispersed. The change from the typical rod-like morphology of CuO to smaller amorphous particles in the mixed oxide suggests that the interaction between CuO and MnO<sub>2</sub> significantly affects the grain formation and structure of the material. This results in a morphological transformation from crystalline to a small amorphous structure with a higher surface area.

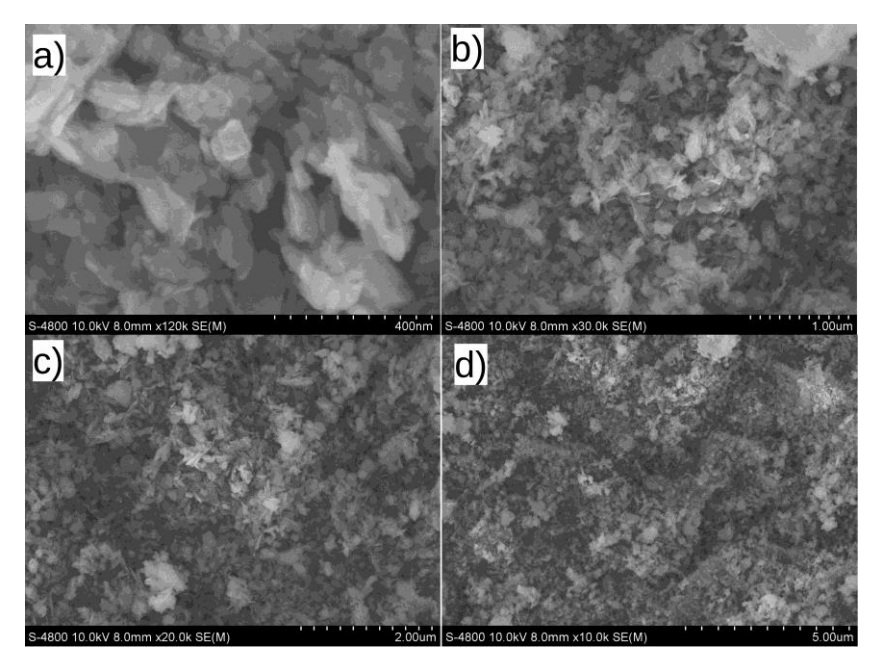


Figure 3. SEM images of CuO oxide

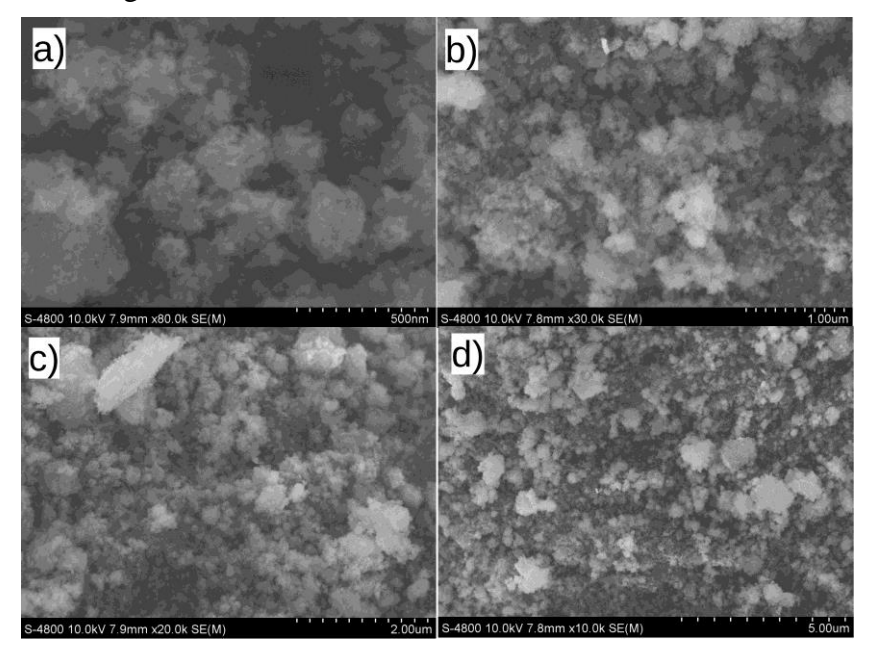
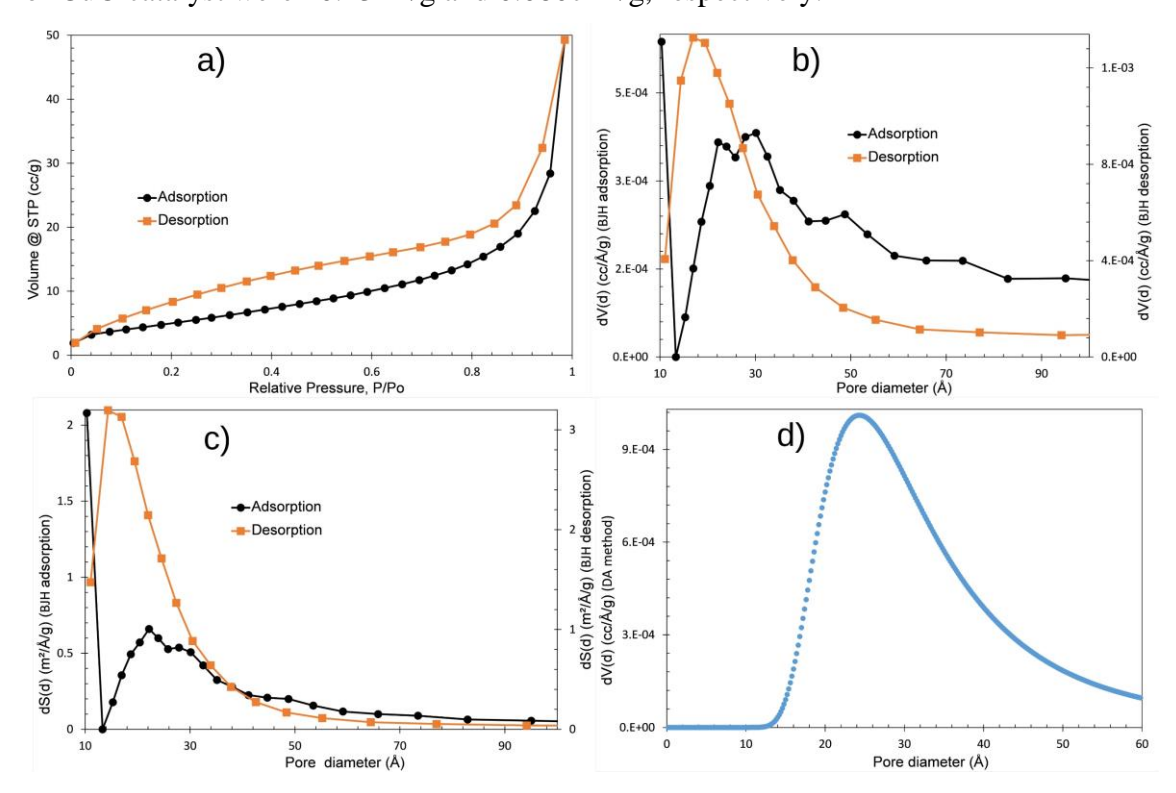


Figure 4. SEM images of 3:1CuO/MnO<sub>2</sub> mixed oxide

# 3.1.3. BET analysis of CuO catalyst

Figure 5a is the  $N_2$  adsorption-desorption isotherm; the curves represent a type IV isotherm (Maji et al., 2010) according to the IUPAC classification. The main characteristic is the appearance of a clear hysteresis loop. Starting from a relative pressure value P/P0 of about 0.4-0.5, there is a sharp increase in the adsorption volume as P/P0 approaches 1. This hysteresis loop, with non-coincident adsorption and desorption curves, is a characteristic sign of capillary condensation in mesopore structures. Where both surface and intra-pore adsorption take place, and the desorption is delayed due to the capillary condensation effect. The analysis of the pore size distribution plots for the CuO material in Figures 5b, c, and d shows that the material is predominantly mesoporous.

Specifically, the BJH plots (Figures 5b and c) all show clear peaks indicating pore sizes concentrated in the range of 20-30Å (2-3nm), with a relatively narrow distribution. The pore size calculated from the BJH desorption curve is usually smaller than that from the BJH adsorption curve due to capillary condensation and pore shape. For "ink-bottle" pores, gas can only escape when the pressure is reduced enough to desorb through the narrowest "neck". Thus, the desorption curve reflects the size of the pore neck. In addition, the surface tension of the condensed liquid film also causes the desorption process to require a lower pressure to break the film, corresponding to a smaller pore size according to the Kelvin formula. In particular, the DA plot (Figure 5d) reinforces this with a peak exactly at around 25Å (2.5nm). The presence of peaks in this range suggests that CuO has a homogeneous mesoporous structure, with relatively uniform pore sizes, which is important for applications involving adsorption or catalysis. The results from the multi-point BET plot and BJH adsorption showed that the surface area and pore volume of CuO catalyst were 20.23m<sup>2</sup>/g and 0.080cm<sup>3</sup>/g, respectively.



*Figure 5.* N<sub>2</sub> adsorption-desorption isotherm (a), pore size distribution vs dV(d) b), pore size distribution vs dS(d), DA method's pore size distribution (d).

## 3.2. Persulfate activation-induced MO degradation

From Figure 6b, it can be seen that the MO adsorption efficiency by these synthesized oxides is quite poor. Specifically, the MO adsorption efficiencies after 120 min at the concentration and volume of MO of 20mg/L and 150mL with the ratios of 1:0, 3:1, 1:1, 1:3, and 0:1 were 13.5%, 11.6%, 10.3%, 7.8%, and 7.6%, respectively. It can be seen that at higher CuO content, the adsorption capacity is higher, but not much different. Figure 6a shows that the zeta potential of CuO (El-Trass et al., 2012) and MO in water is quite negative (-46.5mV and -24.1mV, respectively). Thus, the main reason is believed to be the repulsive electrostatic interaction between the negatively charged adsorbent surfaces and the adsorbate (MO). When both CuO and MO have significant negative zeta

potentials, they tend to repel each other, reducing the ability of MO to adhere to the surface of the materials. This explains why the adsorption efficiency is generally low at all  $CuO/MnO_2$  ratios investigated.

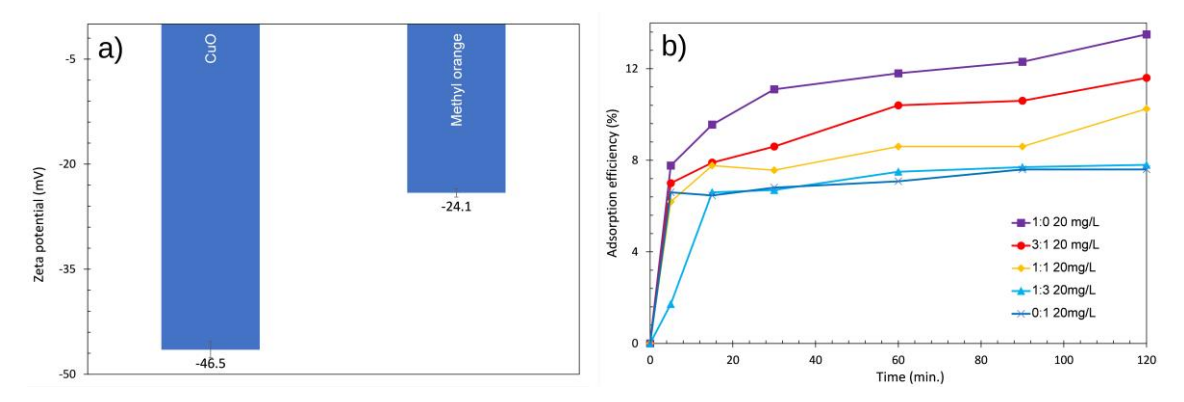


*Figure 6.* The zeta potential of CuO and MO in water (a) and MO adsorption on mixed oxide CuO/MnO<sub>2</sub> (b).

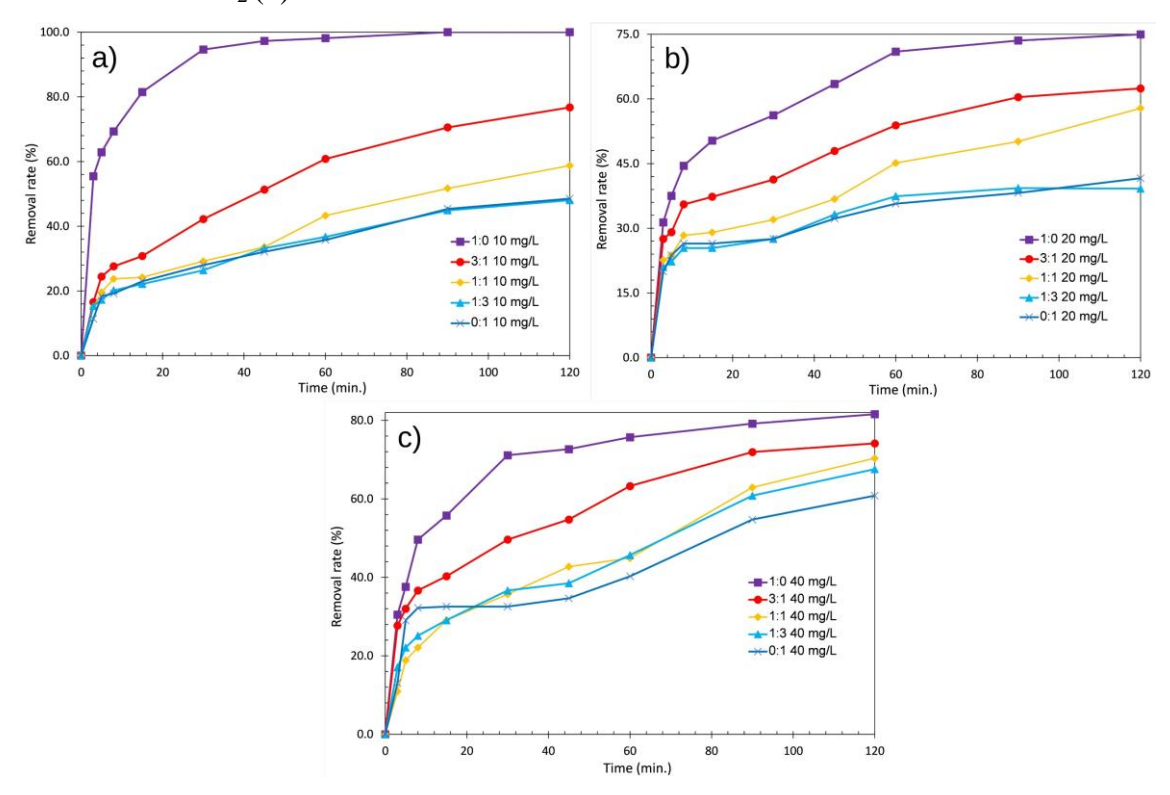


*Figure 7.* The MO degradation efficiencies caused by CuO/MnO<sub>2</sub> catalysts-induced persulfate activation: 10mg/L MO (a), 20mg/L MO (b), and 40mg/L MO (c) solutions.

Figure 7a shows that the MO degradation efficiencies (concentration of 10mg/L) catalyzed by mixed oxides at molar ratios of 1:0, 3:1, 1:1, 1:3, and 0:1 were 100.0%, 76.7%, 58.7%, 48.0%, and 48.5%, respectively. Also in the above order, the MO degradation efficiencies at a concentration of 20mg/L (Figure 7b) were 74.9%, 62.4%, 57.8%, 39.2%, and 41.6%, respectively. Figure 7c shows the MO degradation efficiencies at a concentration of 40mg/L as 81.6%, 74.1%, 70.4%, 67.6%, and 60.8%, respectively (also in the above order). It can be seen that the MO degradation efficiency clearly depends on the initial concentration of MO and the composition ratio of the CuO/MnO<sub>2</sub>

mixed catalyst when activating persulfate. At the same MO concentration (10, 20, and 40mg/L), the catalyst with a ratio of 1:0CuO/MnO<sub>2</sub> always gives the highest degradation efficiency over time, showing the dominant role of CuO in activating persulfate to generate strong free radicals such as SO<sub>4</sub>. When the MnO<sub>2</sub> ratio increases, the degradation efficiency gradually decreases, especially clearly at the ratio of 0:1 (only MnO<sub>2</sub>). This proves that MnO<sub>2</sub> has lower activity than CuO in this reaction system. At the same time, when the MO concentration increases from 10mg/L to 40mg/L, the degradation efficiency generally decreases in all catalyst samples. This reflects the phenomenon of catalytic activity saturation because the number of free radicals generated is not enough to completely decompose the higher initial concentration of MO. In addition, an increasing trend in the yield over time was observed in all samples, but the rate of increase slowed down after 60 min. This suggests that the process gradually reached equilibrium or decreased activity due to persulfate consumption. Therefore, CuO plays a dominant role in the catalyst, and the optimal ratio in the CuO/MnO<sub>2</sub> mixed oxides should be considered to maintain high yield while saving raw materials.

To better understand the MO decomposition reaction kinetics at the above concentrations, we analyzed the change in MO concentration over reaction time following pseudo-first-order (PFO) and pseudo-second-order (PSO) kinetic models (Figure 8). From Figures 8a and b, it can be seen that at an MO concentration of 10mg/L, the MO decomposition catalyzed by CuO best fits PSO ( $R^2 = 0.9732$ ) and that catalyzed by 3:1CuO/MnO<sub>2</sub> best fits PFO ( $R^2 = 0.9909$ ). At MO concentrations of 20mg/L and 40mg/L, CuO catalyst causes MO decomposition following the PSO model with  $R^2$  of 0.9418 and 0.9306, respectively. However, unlike the case of MO concentration of 10mg/L, the  $3:1\text{CuO/MnO}_2$  catalyst induced MO decompositions at concentrations of 20mg/L and 40mg/L follow the PSO model with  $R^2$  of 0.9784 and 0.9861, respectively.

Similarly, we analyzed the MO adsorption kinetics on mixed oxides using pseudo-first-order and pseudo-second-order adsorption kinetic models (Figure 9). The results showed that the adsorption of MO on both CuO and 3:1CuO/MnO<sub>2</sub> catalysts was best fitted by the PSO adsorption kinetic model (Figure 9b) with R<sup>2</sup> of 0.9974 and 0.9974, respectively.

The MO adsorption and degradation kinetics models were based on the following equations (Ball, 1998; Revellame et al., 2020):

PFO adsorption kinetic model:  $ln(q_e - q_t) = lnq_e - k_{1a}t$  (2)

Where  $q_t$  is the amount of adsorbed substance at time t (mg/g),  $q_e$  is the amount of adsorbed substance at equilibrium (mg/g), and  $k_{1a}$  is the PFO rate constant (1/min)

PSO adsorption kinetic model: 
$$\frac{t}{q_t} = \frac{1}{k_{2a}q_e^2} + \frac{t}{q_e}$$
 (3)

Where k<sub>2a</sub> is the PSO rate constant (g/mg.min)

PFO reaction kinetic model:  $lnC_t = lnC_0 - k_{1r}t$  (4)

Where  $C_0$  is the initial concentration of reactants (mg/L),  $C_t$  is the reactant concentration at time t (mg/L), and  $k_{1r}$  is the PFO reaction rate constant (1/min).

PSO reaction kinetic model: 
$$\frac{1}{c_t} = \frac{1}{c_0} + k_{2r}t$$
 (5)

Where  $k_{2r}$  is the PSO reaction rate constant (L/mg.min).

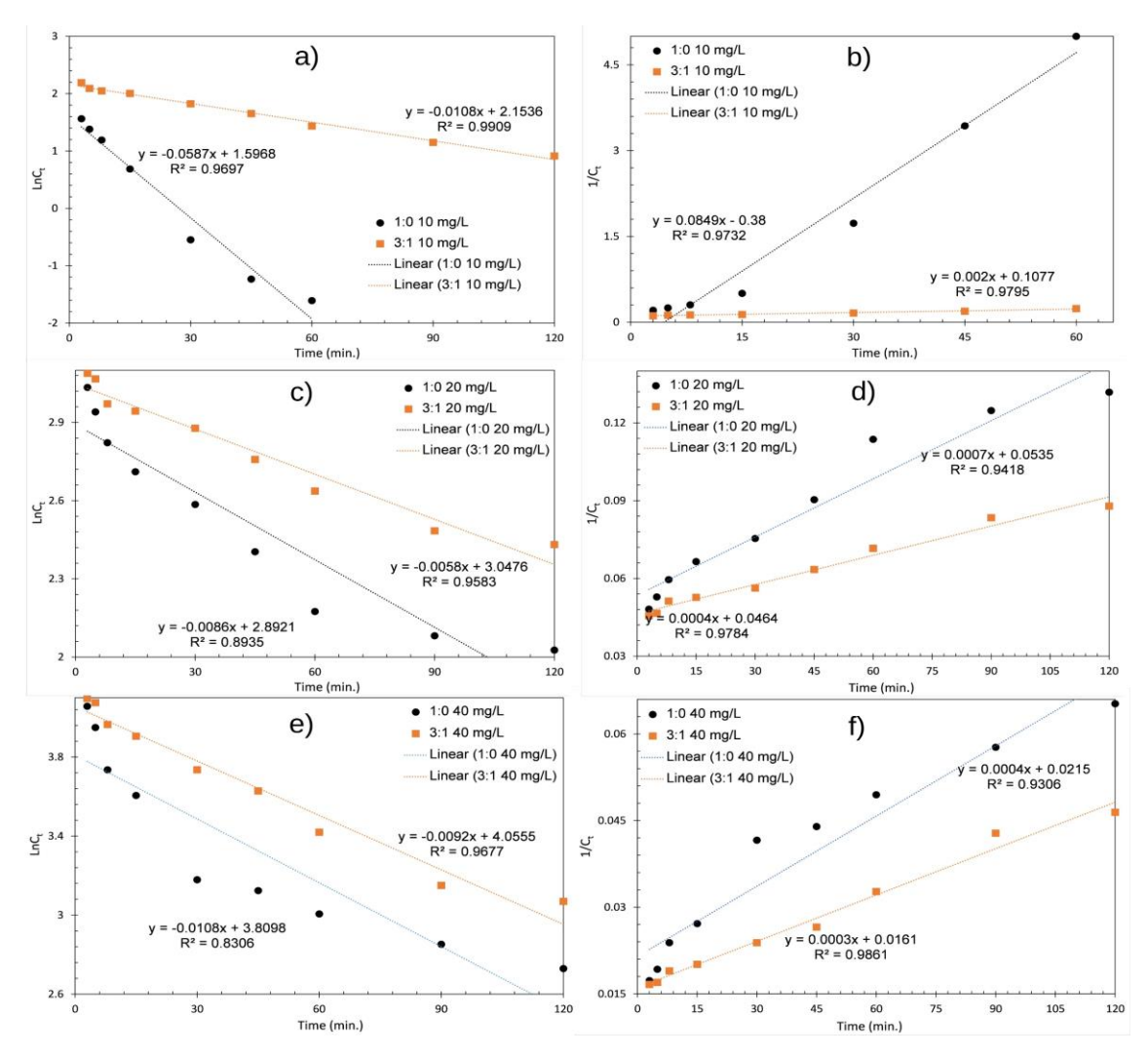


*Figure 8.* 10mg/L MO: PFO (a) and PSO (b) kinetic model; 20mg/L MO: PFO (c) and PSO (d) kinetic model; and 40mg/L MO: PFO (e) and PSO (f) kinetic model.

TABLE 1. PSO reaction rate constants of MO degradations

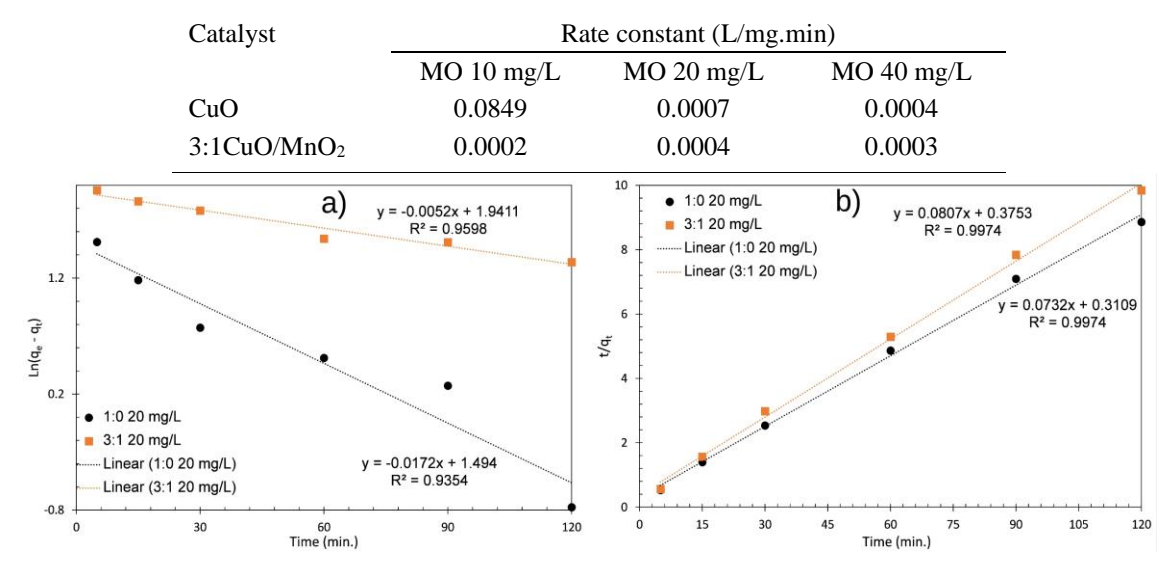


Figure 9. The PFO (a) and PSO (b) kinetic models of MO adsorption

**Table 2.** Rate constants of MO adsorptions

Catalyst	PFO rate constant (1/min)	PSO rate constant (g/mg.min)
CuO	0.0172	0.0732
3:1CuO/MnO <sub>2</sub>	0.0052	0.0807

#### 4. Conclusion

In conclusion, CuO/MnO<sub>2</sub> mixed metal oxides were successfully synthesized. FTIR spectra of CuO and 3:1CuO/MnO<sub>2</sub> confirmed the presence of characteristic peaks of the oxide and the interaction between metals in its structure. SEM images showed that CuO particles were rod-shaped with a length of 100nm and a width of about 30nm; whereas, 3:1CuO/MnO<sub>2</sub> particles were very small in size and appeared to be amorphous. BET analyses of the CuO sample showed that its specific surface area and pore size were 20.23m²/g and 20-30Å, respectively. The zeta potentials of CuO and MO in water were both highly negative, explaining the poor adsorption of MO onto the mixed oxides (maximum 13.5%). In contrast, the MO degradation catalyzed by the oxides was much more efficient. The MO decomposition at initial concentrations of 40mg/L catalyzed by CuO and 3:1CuO/MnO<sub>2</sub> was 81.6% and 74.1%, respectively. In addition, the adsorption of MO onto oxides followed pseudo-second-order kinetics. The MO decomposition at different initial concentrations mainly followed pseudo-second-order reaction kinetics. It can be seen that CuO has better catalytic ability to decompose and adsorb MO than MnO<sub>2</sub>.

# Acknowledgments

This student's research is funded by Thu Dau Mot University, Ho Chi Minh City, Vietnam, under grant number 2024000509.

#### References

- Ball, D. (1998). Kinetics of Consecutive Reactions: First Reaction, First-Order; Second Reaction, Zeroth Order. *Journal of Chemical Education*, 75(7), 917.
- Chang, Y., & Zeng, H. C. (2004). Controlled Synthesis and Self-Assembly of Single-Crystalline CuO Nanorods and Nanoribbons. *Crystal Growth & Design*, 4(2), 397-402.
- El-Trass, A., ElShamy, H., El-Mehasseb, I., & El-Kemary, M. (2012). CuO nanoparticles: Synthesis, characterization, optical properties and interaction with amino acids. *Applied Surface Science*, 258(7), 2997-3001.
- Fernandes, D. M., Silva, R., Hechenleitner, A. A. W., Radovanovic, E., Melo, M. A. C., & Pineda, E. A. G. (2009). Synthesis and characterization of ZnO, CuO and a mixed Zn and Cu oxide. *Materials Chemistry and Physics*, 115(1), 110-115.
- Huang, J., & Zhang, H. (2019). Mn-based catalysts for sulfate radical-based advanced oxidation processes: A review. *Environment International*, *133*, 105141.
- Liu, X., Huang, Y., Zhao, P., Meng, X., & Astruc, D. (2020). Precise Cu Localization-Dependent Catalytic Degradation of Organic Pollutants in Water. *ChemCatChem*, *12*(1), 175-180.
- Luo, X., Liang, H., Qu, F., Ding, A., Cheng, X., Tang, C. Y., & Li, G. (2018). Free-standing hierarchical α-MnO2@CuO membrane for catalytic filtration degradation of organic pollutants. *Chemosphere*, 200, 237-247.

- Maji, S. K., Mukherjee, N., Mondal, A., Adhikary, B., & Karmakar, B. (2010). Chemical synthesis of mesoporous CuO from a single precursor: Structural, optical and electrical properties. *Journal of Solid State Chemistry*, 183(8), 1900-1904.
- Oyekunle, D. T., Gendy, E. A., Ifthikar, J., & Chen, Z. (2022). Heterogeneous activation of persulfate by metal and non-metal catalyst for the degradation of sulfamethoxazole: A review. *Chemical Engineering Journal*, 437, 135277.
- Revellame, E. D., Fortela, D. L., Sharp, W., Hernandez, R., & Zappi, M. E. (2020). Adsorption kinetic modeling using pseudo-first order and pseudo-second order rate laws: A review. *Cleaner Engineering and Technology*, *1*, 100032.
- Wang, B., & Wang, Y. (2022). A comprehensive review on persulfate activation treatment of wastewater. *Science of The Total Environment*, 831, 154906.
- Wu, R., Hu, X., Li, Y., Li, Y., Cai, Y., Jiang, P., & Yu, B. (2023). Efficient activation of peroxymonosulfate by amorphous MnO2/α-Fe2O3 for the degradation of organic pollutants. *Chemical Engineering Journal*, 473, 145011.
- Yang, Y., Zhang, P., Hu, K., Duan, X., Ren, Y., Sun, H., & Wang, S. (2021). Sustainable redox processes induced by peroxymonosulfate and metal doping on amorphous manganese dioxide for nonradical degradation of water contaminants. *Applied Catalysis B: Environmental*, 286, 119903.
- Zhao, M., Xu, R., Chen, Z., Gao, Z., Zheng, S., & Song, H. (2022). Kinetics and mechanisms of diniconazole degradation by α-MnO2 activated peroxymonosulfate. *Separation and Purification Technology*, 281, 119850.
- Zhi, D., Lin, Y., Jiang, L., Zhou, Y., Huang, A., Yang, J., & Luo, L. (2020). Remediation of persistent organic pollutants in aqueous systems by electrochemical activation of persulfates: A review. *Journal of Environmental Management*, 260, 110125.
- Zhu, S., Ho, S.-H., Jin, C., Duan, X., & Wang, S. (2020). Nanostructured manganese oxides: natural/artificial formation and their induced catalysis for wastewater remediation. *Environmental Science: Nano*, 7(2), 368-396.